AIP Advances

The competition between the hydrodynamic instability from noise and magnetorotational instability in the Keplerian disks

Cite as: AIP Advances **12**, 055228 (2022); https://doi.org/10.1063/5.0095282
Submitted: 09 December 2021 • Accepted: 11 April 2022 • Published Online: 25 May 2022

Subham Ghosh and Banibrata Mukhopadhyay

The competition between the hydrodynamic instability from noise and magnetorotational instability in the Keplerian disks

Cite as: AIP Advances 12, 055228 (2022); doi: 10.1063/5.0095282
Submitted: 9 December 2021 • Accepted: 11 April 2022 •
Published Online: 25 May 2022

Subham Ghosh[a] and Banibrata Mukhopadhyay[b]

AFFILIATIONS

Department of Physics, Indian Institute of Science, Bangalore 560012, India

[a]Author to whom correspondence should be addressed: ghosh.pqr@gmail.com and subham@iisc.ac.in
[b]E-mail: bm@iisc.ac.in

ABSTRACT

We venture for the comparison between growth rates for magnetorotational instability (MRI) and hydrodynamics instability in the presence of an extra force in the local Keplerian accretion flow. The underlying model is described by the Orr–Sommerfeld and Squire equations in the presence of rotation, magnetic field, and an extra force, plausibly noise with a nonzero mean. We obtain MRI using the Wentzel–Kramers–Brillouin approximation without extra force for a purely vertical magnetic field and vertical wavevector of the perturbations. Expectedly, MRI is active within a range of magnetic field, which changes depending on the perturbation wavevector magnitude. Next, to check the effect of noise on the growth rates, a quartic dispersion relation has been obtained. Among those four solutions for the growth rate, the one that reduces to the MRI growth rate at the limit of vanishing mean of noise in the MRI active region of the magnetic field is mostly dominated by MRI. However, in the MRI inactive region, in the presence of noise, the solution turns out to be unstable, which is almost independent of the magnetic field. Another growth rate, which is almost complementary to the previous one, leads to stability at the limit of vanishing noise. The remaining two growth rates, which correspond to the hydrodynamical growth rates at the limit of the vanishing magnetic field, are completely different from the MRI growth rate. More interestingly, the latter growth rates are larger than that of the MRI. If we consider viscosity, the growth rates decrease depending on the Reynolds number.

I. INTRODUCTION

The accretion disk is one of the exotic objects in astrophysics. As the name suggests, they form a disk-like shape due to the accretion of matter with angular momentum around a center by unleashing enormous gravitational energy through radiation. They are ubiquitous. From around the center of the galaxies to the formation of planets, from the binary system to the ring of Saturn, they prevail at various length scales. The physics related to the accretion disks is also exotic. There have been a lot of studies regarding the phenomena related to the accretion disks, and it still continues. However, still there are some open questions in the field of accretion disks. One of those is how, in the first place, the accretion disk forms, i.e., how the matter falls in, losing the angular momentum and eventually reaches the central object, particularly where the molecular viscosity is negligible. We attempt to address this question in this work.

To match with the observational evidences,[1] the accretion flow has to be turbulent.[2] However, the accretion flow in the Keplerian accretion disk, where the centrifugal force almost balances the gravity, is Rayleigh (centrifugally) stable, i.e., the infinitesimal perturbation eventually dies down. The route to turbulence, therefore, is essential to find. In 1991, Balbus and Hawley[3] proposed the idea of an ideal magnetohydrodynamical (MHD) instability following Velikhov[4] and Chandrasekhar:[5] magnetorotational instability (MRI). The interplay between the weak magnetic field and the rotation of the fully ionized plasma gives rise to the MRI. It is a widespread mechanism leading to turbulence and explaining the transport of angular momentum in accretion disks. This is because

it grows within the dynamical timescale with very minimum requirements: weak magnetic field so that the corresponding magnetic pressure is smaller than the hydrodynamical pressure and a radially decreasing angular velocity in contrast to the radially decreasing specific angular momentum as the Rayleigh stability criterion.[6] Despite its popularity in the accretion disk community and tremendous success in explaining various accretion phenomena over the years, the MRI is not out of caveats. When the temperature is low, the fluid and the magnetic field do not get coupled well due to inefficient ionization. Consequently, the nonideal MHD effects come into the picture. Due to the stabilizing effects of Ohmic resistivity on the linear instability, there are many regions in protoplanetary disks where MRI gets suppressed.[7,8] The additional inclusion of ambipolar diffusion makes this scenario worse.[9]

In order to explain the angular momentum transport, magnetized disk winds have been considered as an alternative to MRI turbulence.[10,11] If the toroidal component of the magnetic field is beyond the critical value, MRI gets suppressed locally[12] and globally.[13] Instead, there arise different MHD instabilities. Moreover, due to the non-normality of the underlying system, it has been argued that the magnetic transient growth[14] brings nonlinearity and hence plausible turbulence faster than MRI for the flows with the Reynolds number (Re) beyond 10^9. Since Re in accretion disk[15] is much larger than this value, MRI is questionable in systems with large Re. It, therefore, would be an enthralling venture to look for the instability mechanisms of hydrodynamical origins.

A lot of efforts have been put forward to understand the angular momentum transport in accretion disks in the laboratory, i.e., through the table top experiments and simulations. To do so, the accretion disk-like environment, i.e., the Keplerian angular velocity, has been created in the experiments. In the experimental context, the Taylor–Couette flow[16] has been considered. Its crude description is the following. It has two concentric cylinders and fluid in between. By moving the cylinders, the fluid is kept in motion. The flow parameters, i.e., the velocity, angular velocity, and Re, are controlled by the speed of both the cylinders.[17] Although the exploration of the transport of angular momentum in accretion disk through laboratory was started by Richard and Zahn[18] in 1999, based on the key experimental results, there are mainly two groups in the community: one (group 1) who obtained hydrodynamic turbulence[19–21] for the Keplerian angular velocity profile and the other one (group 2) who did not obtain any hydrodynamic turbulence[22] for the same. All the experiments reached the equivalently same Re to draw their conflicting conclusions. Although they obtained the same Re, the two groups have different experimental devices. group 1 did the experiment with a tall and narrow device, while group 2 used a small and wide apparatus. These kinds of geometrical differences in the apparatus affect the critical Re of the corresponding flows remarkably.[18,23] For the same reason, turbulence is hard to reach in the case of a wide apparatus. It could be plausible for group 2 that they operated the apparatus at the verge of the critical Re required for the transition to turbulence or below the critical Re so that they did not reach the turbulent regime. Although, in reality, there is no rigid axial boundary in accretion disks, due to the finite size of the apparatus, each group differently implemented the axial boundaries. To check the effect of these axial boundaries on the flow, a direct numerical simulation,[24] with very small Re compared to the experiments due to the computational constraint, was performed in the equivalent setup of the experiments done by both the groups. The simulations of both the experiments show that the flows become turbulent mainly due to the presence of the boundaries. Hence, the effects of boundaries, i.e., the finite size of the apparatus, have important roles in bringing turbulence. From the theoretical, numerical, and experimental points of view, the current status of the field is still far from settling down.

Keeping in mind the nonmagnetic Keplerian flow, an alternative approach of linear transient growth[25–29] has been also proposed. Due to the non-selfadjoint property of the underlying differential operator, the total energy[30] of the linear perturbations in the shear flow becomes significantly large for a short time before their eventual decay. Although its tremendous success is in explaining the subcritical transition to turbulence in the laboratory shear flows, the authors of Refs. 28, 31, and 32 questioned for the corresponding sustained turbulence in the Keplerian flow. However, several orders of magnitude discrepancies exist between the current computational resolution and the Re of the accretion disk. Nevertheless, we encounter the problem from the hydrodynamical point of view but in the presence of an extra force. Considering this extra force to be the white noise with a zero mean, the multi-mode analysis of the Keplerian flow has been studied.[33,34] We instead follow the idea and methodology put forwarded by Mukhopadhyay and Chattopadhyay.[15] Recently, the authors of Refs. 35–38 argued that if the white noise has a nonzero mean, the Keplerian flow effectively becomes linearly unstable. The origin of the extra force in the context of accretion flow, as merely mentioned by Ioannou and Kakouris,[33] could be the neglected nonlinear terms during the linear analysis, supernova explosions, etc. However, the other plausible models for its origin, as proposed explicitly and rigorously by Ghosh and Mukhopadhyay[36] very recently, could be the dust–grain interaction in protoplanetary disks, feedback from the outflow/jet on the accretion disks, etc. Nevertheless, the comparison between the growth rates of hydrodynamical instability in the presence of an extra force and that of the MRI has never been studied. Although there could be different models for the extra force,[33,36] we, however, restrict ourselves to the white noise with nonzero mean as the extra force in this work. This study has its own significance because the presence of noise is not limited[35,36] to the nonmagnetic Keplerian flow. The presence of noise, in fact, is quite ubiquitous in any Keplerian flow as argued by Nath and Mukhopadhyay[35] and later by Ghosh and Mukhopadhyay.[36] Hence, it is very important to compare these two growth rates to check whether they come in unison or one opposes the other. In other words, the growth rate corresponding to the hydrodynamical instability is in the favorable parameter space for MRI. If the growth rate of the hydrodynamical instability is comparable to that of the MRI, we can say that irrespective of the magnetic field, the accretion flow is linearly unstable. Hence, nonlinearity and turbulence eventually could be the inevitable fate of the magnetic or nonmagnetic Keplerian flow.

This paper is organized as follows: In Sec. II, we first formulate the problem in the local shearing box situated at a local patch of the accretion disk. In the local box, the governing equations to describe the linearly perturbed background flow are the magnetic Orr–Sommerfeld and Squire equations in the presence of an extra force and the Coriolis force. The corresponding background magnetic and velocity fields are also described here. With these equations, in the absence of the extra force, we obtain a dispersion

relation neglecting the hydrodynamic and magnetic viscosities to obtain the criteria for centrifugal instability (CI) and MRI in Sec. III. The effect of the force is described in Sec. IV, where the dispersion relation in the presence of noise but in the absence of any kinds of viscosity is obtained. Note that if the external force is not stochastic rather deterministic, a similar scenario can also be implemented. The solutions for that dispersion relation have been studied extensively without magnetic field in Sec. IV A and with magnetic field in Sec. IV B. In Sec. V, we include the effect of the hydrodynamic viscosity on the growth rates. We conclude in Sec. VI that depending on the extra force, the hydrodynamic growth rate in the favorable parameter zone for MRI becomes greater than that of the MRI. For other parameters, which lead to the suppression of MRI, it is the hydrodynamical instability that makes the flow unstable and plausibly further turbulent. Hence, the presence of noise in the flow is enough to make the underlying flow unstable.

II. FORMALISM

We refer to the local patch of the Keplerian accretion disk, where we do the whole analysis. For the detailed description of the local formulation, see Refs. 28, 39, and 40. The governing equations of the perturbed flow are the magnetic Navier–Stokes equation in the presence of rotation and noise, the magnetic induction equation with the constraints of incompressibility[14,29] due to the local nature of the flow, and the no-magnetic monopole. We, however, recast the governing equations into magnetic Orr–Sommerfeld and Squire equations (see the Appendix of Mukhopadhyay and Chattopadhyay[15] for the detailed derivation). The background and perturbed velocities are $\mathbf{U}_0 = (0, -x, 0)$[6,28,38] and (u, v, w), respectively. For the present purpose, the background and perturbed magnetic fields are $\mathbf{B}_0 = (B_{0x}, B_{0y}, B_{0z})$ and (B_x, B_y, B_z), respectively. Hence, taking into account the above-mentioned background and perturbed quantities, the magnetized Orr–Sommerfeld and Squire equations become

$$\left(\frac{\partial}{\partial t} - x\frac{\partial}{\partial y}\right)\nabla^2 u + \frac{2}{q}\frac{\partial \zeta}{\partial z} - \frac{1}{4\pi}(\boldsymbol{B}_0 \cdot \nabla)\nabla^2 B_x = \frac{1}{Re}\nabla^4 u + \eta_1, \quad (1a)$$

$$\left(\frac{\partial}{\partial t} - x\frac{\partial}{\partial y}\right)\zeta + \left(1 - \frac{2}{q}\right)\frac{\partial u}{\partial z} - \frac{1}{4\pi}(\boldsymbol{B}_0 \cdot \nabla)\zeta_B = \frac{1}{Re}\nabla^2 \zeta + \eta_2, \quad (1b)$$

$$\left(\frac{\partial}{\partial t} - x\frac{\partial}{\partial y}\right)B_x - (\boldsymbol{B}_0 \cdot \nabla)u = \frac{1}{Rm}\nabla^2 B_x, \quad (1c)$$

$$\left(\frac{\partial}{\partial t} - x\frac{\partial}{\partial y}\right)\zeta_B - (\boldsymbol{B}_0 \cdot \nabla)\zeta - \frac{\partial}{\partial z}B_x = \frac{1}{Rm}\nabla^2 \zeta_B, \quad (1d)$$

where $\eta_{1,2}$ are the extra force; $\zeta = \partial w/\partial y - \partial v/\partial z$ and $\zeta_B = \partial B_z/\partial y - \partial B_y/\partial z$ are the x-component of vorticity and magnetic vorticity, respectively; Re and Rm are the Reynolds and magnetic Reynolds numbers, respectively; and q is the rotation parameter describing the radial dependence (r) of the angular frequency (Ω) of the fluid element around the central object, given by $\Omega \propto r^{-q}$.

We have to write down Eqs. (1a)–(1d) in the Fourier space in the due course of calculation. For that, our convention of the Fourier transformation and the inverse Fourier transformation are, respectively,

$$A(\mathbf{r}, t) = \int \tilde{A}_{\mathbf{k},\omega} e^{i(\mathbf{k}\cdot\mathbf{r} - \omega t)} d^3k\, d\omega \quad (2a)$$

and

$$\tilde{A}_{\mathbf{k},\omega} = \left(\frac{1}{2\pi}\right)^4 \int A(\mathbf{r}, t) e^{-i(\mathbf{k}\cdot\mathbf{r} - \omega t)} d^3x\, dt, \quad (2b)$$

where A can be any one of $u, \zeta, B_x, \zeta_B, \eta_1$, and η_2; $\mathbf{k}$ and ω are the wavevector and the corresponding frequency of the perturbation in the Fourier space such that in Cartesian coordinates, $\mathbf{k} \equiv (k_x, k_y, k_z)$ and $|\mathbf{k}| = k$; and $\mathbf{r}$ is the position vector, and in Cartesian coordinates, $\mathbf{r} \equiv (x, y, z)$.

The boundary conditions to solve Eqs. (1a)–(1d) are

$$u = \frac{\partial u}{\partial x} = \zeta = B_x = \frac{\partial B_x}{\partial x} = \zeta_B = 0, \text{ at } x = \pm 1. \quad (3)$$

In the Fourier space, the above equations reduce to

$$-k_y k^2 \frac{\partial \tilde{u}_{\mathbf{k},\omega}}{\partial k_x} + \left(i\omega k^2 - 2k_x k_y - \frac{k^4}{Re}\right)\tilde{u}_{\mathbf{k},\omega} + \frac{2ik_z}{q}\tilde{\zeta}_{\mathbf{k},\omega} + \frac{ik^2}{4\pi}(\mathbf{B}_0 \cdot \mathbf{k})\tilde{B}_{x;\mathbf{k},\omega} = m_1 \delta(\mathbf{k})\delta(\omega), \quad (4a)$$

$$k_y \frac{\partial \tilde{\zeta}_{\mathbf{k},\omega}}{\partial k_x} + ik_z\left(1 - \frac{2}{q}\right)\tilde{u}_{\mathbf{k},\omega} + \left(\frac{k^2}{Re} - i\omega\right)\tilde{\zeta}_{\mathbf{k},\omega} - \frac{i}{4\pi}(\mathbf{B}_0 \cdot \mathbf{k})\tilde{\zeta}_{B;\mathbf{k},\omega} = m_2 \delta(\mathbf{k})\delta(\omega), \quad (4b)$$

$$k_y \frac{\partial}{\partial k_x}\tilde{B}_{x;\mathbf{k},\omega} + \left(\frac{k^2}{Rm} - i\omega\right)\tilde{B}_{x;\mathbf{k},\omega} - i(\mathbf{B}_0 \cdot \mathbf{k})\tilde{u}_{\mathbf{k},\omega} = 0, \quad (4c)$$

$$k_y \frac{\partial}{\partial k_x}\tilde{\zeta}_{B;\mathbf{k},\omega} + \left(\frac{k^2}{Rm} - i\omega\right)\tilde{\zeta}_{B;\mathbf{k},\omega} - i(\mathbf{B}_0 \cdot \mathbf{k})\tilde{\zeta}_{\mathbf{k},\omega} - ik_z \tilde{B}_{x;\mathbf{k},\omega} = 0. \quad (4d)$$

We choose the solutions of Eqs. (1a)–(1d) to be $\psi = \psi(x)e^{i(\boldsymbol{\alpha}\cdot\mathbf{r} - \beta t)}$, where ψ can be any of u, ζ, B_x, and ζ_B; $\boldsymbol{\alpha} = (\alpha_1, \alpha_2, \alpha_3)$ is the wave vector; and β is the frequency. In general, β is complex. However, according to our convention, if the imaginary part of β, i.e., $Im(\beta)$, is positive, then the perturbation grows with time and, hence, makes the flow unstable. In the Fourier space, these solutions become

$$\tilde{\psi}_{\mathbf{k},\omega} = \left(\frac{1}{2\pi}\right)^4 \int_{-\infty}^{\infty} \psi(x) e^{i(\boldsymbol{\alpha}\cdot\mathbf{r} - \beta t)} e^{-i(\mathbf{k}\cdot\mathbf{r} - \omega t)} d^3x dt = \frac{1}{2\pi}\delta(\alpha_2 - k_y)\delta(\alpha_3 - k_z)\delta(\beta - \omega)\int_{-\infty}^{\infty} \psi(x) e^{i(\alpha_1 - k_x)x} dx.$$

To obtain the dispersion relation, we integrate Eqs. (4a)–(4d) with respect to $\mathbf{k}$ and ω and obtain the following equations. In the due

process, we have neglected the second and higher order derivatives. Thence, the corresponding equations are

$$\left(i\beta\alpha^2 - \frac{\alpha^4}{Re}\right)u(0) + 2i\alpha_1\left(\frac{2\alpha^2}{Re} - i\beta\right)u'(0) + \frac{2i\alpha_3}{q}\zeta(0) + \frac{i}{4\pi}\left[(\mathbf{B}_0\cdot\boldsymbol{\alpha})(\alpha^2 B_x(0) - 2i\alpha_1 B_x'(0))\right] = m_1, \tag{5a}$$

$$i\alpha_3\left(1 - \frac{2}{q}\right)u(0) + \left(\frac{\alpha^2}{Re} - i\beta\right)\zeta(0) - \frac{2i\alpha_1}{Re}\zeta'(0) - \frac{i}{4\pi}(\mathbf{B}_0\cdot\boldsymbol{\alpha})\zeta_B(0) = m_2, \tag{5b}$$

$$\left(\frac{\alpha^2}{Rm} - i\beta\right)B_x(0) - \frac{2i\alpha_1}{Rm}B_x'(0) - i(\mathbf{B}_0\cdot\boldsymbol{\alpha})u(0) = 0, \tag{5c}$$

$$\left(\frac{\alpha^2}{Rm} - i\beta\right)\zeta_B(0) - \frac{2i\alpha_1}{Rm}\zeta_B'(0) - i(\mathbf{B}_0\cdot\boldsymbol{\alpha})\zeta(0) - i\alpha_3 B_x(0) = 0. \tag{5d}$$

A. Background magnetic field

Before proceeding further, we have to specify the background magnetic field, B_0, like we know about U_0. The induction equation in dimensionless unit, in general, is

$$\frac{\partial\boldsymbol{\mathcal{B}}}{\partial t} = \nabla\times(\mathbf{V}\times\boldsymbol{\mathcal{B}}) + \frac{1}{Rm}\nabla^2\boldsymbol{\mathcal{B}}, \tag{6}$$

where $\boldsymbol{\mathcal{B}}$ and $\mathbf{V}$ are arbitrary magnetic and velocity field vectors, respectively. If we assume the background magnetic field to be constant over space and time, then Eq. (6) for background quantities becomes

$$\nabla\times(\boldsymbol{U}_0\times\mathbf{B}_0) = (\mathbf{B}_0\cdot\nabla)\mathbf{U}_0 - (\mathbf{U}_0\cdot\nabla)\mathbf{B}_0 = 0. \tag{7}$$

For $\mathbf{U}_0 = (0, -x, 0)$, Eq. (7) becomes

$$-B_{0x}\mathbf{j} + x\frac{\partial\mathbf{B}_0}{\partial y} = 0, \tag{8}$$

where $\mathbf{j}$ is the unit vector along the y-direction in Cartesian coordinates. We, therefore, obtain that for the constant background magnetic field, $B_{0x} = 0$, and hence, $\mathbf{B}_0 = (0, B_{0y}, B_{0z})$. In this work, we shall be, however, focusing on the vertical magnetic field, i.e., $\mathbf{B}_0 = (0, 0, B_{0z})$.

III. THE CENTRIFUGAL INSTABILITY AND MAGNETOROTATIONAL INSTABILITY

It is always interesting to obtain CI and MRI following our formalism. We, in fact, obtain the corresponding dispersion relations out of Eqs. (5a)–(5d) omitting noise. Our primary interest is for the vertical wave vector, i.e., $\boldsymbol{\alpha} = (0, 0, \alpha_3)$. We also neglect the effect of viscosity for the time being. Eventually, in this work itself, we include all of them one by one in the due course of study. Considering all these, Eqs. (5a)–(5d) become

$$\begin{aligned} i\beta\alpha_3^2 u(0) + \frac{2i\alpha_3}{q}\zeta(0) + \frac{i\alpha_3^3 B_{0z}B_x(0)}{4\pi} &= 0,\\ i\alpha_3\left(1 - \frac{2}{q}\right)u(0) - i\beta\zeta(0) - \frac{i}{4\pi}B_{0z}\alpha_3\zeta_B(0) &= 0,\\ -i\beta B_x(0) - iB_{0z}\alpha_3 u(0) &= 0,\\ -i\beta\zeta_B(0) - iB_{0z}\alpha_3\zeta(0) - i\alpha_3 B_x(0) &= 0. \end{aligned} \tag{9}$$

For the nontrivial solutions of the above system of linear equations, we obtain the following dispersion relation:

$$16\pi^2\beta^4 - 8\pi\left[B_{0z}^2\alpha_3^2 - \left(4\pi\left(\frac{1}{q} - \frac{2}{q^2}\right)\right)\right]\beta^2 + B_{0z}^4\alpha_3^4 - \frac{8\pi B_{0z}^2\alpha_3^2}{q} = 0. \tag{10}$$

For the centrifugal instability,[16,41] we get rid of the magnetic field from Eq. (10). The nontrivial solutions are

$$\beta = \pm\frac{\sqrt{2}}{q}\sqrt{2-q}. \tag{11}$$

It tells us that for $q > 2$, the flow becomes unstable. If we keep the magnetic field and get rid of the rotation parameter (q), we would obtain magneto-hydrodynamical (MHD) waves with frequency

$$\beta = \pm\frac{B_{0z}\alpha_3}{2\sqrt{\pi}}. \tag{12}$$

These waves are called Alfven waves with Alfven speed, $V_A = B_{0z}/2\sqrt{\pi}$.

If we keep both rotation and the magnetic field, from Eq. (10), we obtain that $q > 0$ for instability, i.e., negative β^2 for an arbitrarily small α_3. This is MRI. Equation (10) shows that β has four solutions. However, among them, only one provides instability. Figure 1 shows the variation of $Im(\beta)$ as a function of B_{0z} for various combinations between $q = 1, 1.5$, and 2 and $\alpha_3 = 1, 5, 10$. There, we find that as the magnitude of B_{0z} increases, first $Im(\beta)$ also increases and reaches a maximum value of 0.5,[6] and then it decreases. It also says that for a fixed α_3, as q increases, the domain of B_{0z} giving rise to positive $Im(\beta)$ decreases. On the other hand, for a fixed q, the increment of α_3 decreases the window of B_{0z}, which gives rise to positive $Im(\beta)$. Between these effects of α_3 and q, the increment of α_3 for a fixed q affects the flow more severely.

IV. THE EFFECT OF EXTRA FORCE

In the presence of an extra force, the vertical magnetic field, and the vertical wavevector, Eqs. (5a)–(5d) become

$$\begin{aligned} i\beta\alpha_3^2 u(0) + \frac{2i\alpha_3}{q}\zeta(0) + \frac{i\alpha_3^3 B_{0z}B_x(0)}{4\pi} &= m_1,\\ i\alpha_3\left(1 - \frac{2}{q}\right)u(0) - i\beta\zeta(0) - \frac{i}{4\pi}B_{0z}\alpha_3\zeta_B(0) &= m_2,\\ -i\beta B_x(0) - iB_{0z}\alpha_3 u(0) &= 0,\\ -i\beta\zeta_B(0) - iB_{0z}\alpha_3\zeta(0) - i\alpha_3 B_x(0) &= 0. \end{aligned} \tag{13}$$

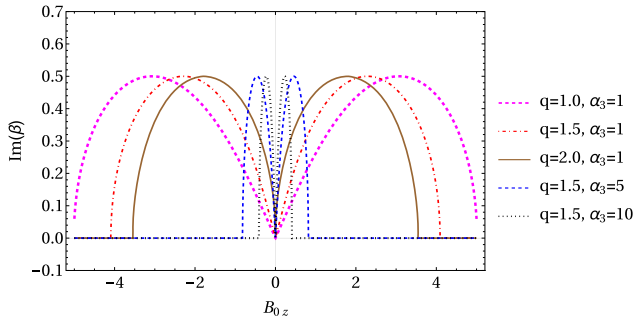

FIG. 1. Variation of $Im(\beta)$ of the unstable solution from Eq. (10) as a function of B_{0z} for various combinations of q and α_3 for inviscid flow.

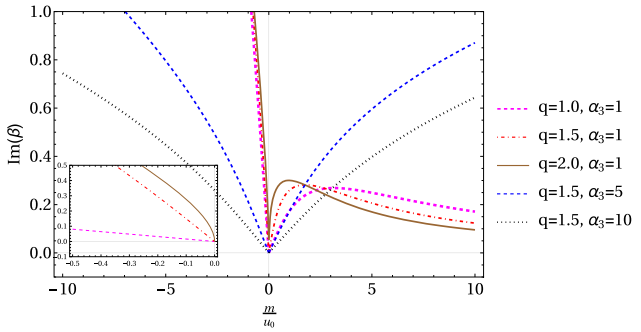

FIG. 2. Variation of $Im(\beta)$ of the unstable solution from Eq. (15) as a function of m/u_0 for various combinations of q and α_3 for inviscid flow.

For simplicity, if we consider $m_1 = m_2 = m$ and write $u(0)$ as u_0, the dispersion relation from Eq. (13) becomes

$$\frac{m}{u_0}\left(4\pi\alpha_3^2 B_{0z}^2\beta - 16\pi^2\beta^3\right) = \frac{8i\pi B_{0z}^2\alpha_3^4}{q} - i\alpha_3^6 B_{0z}^4 + \frac{32\pi^2\alpha_3\beta^2}{q}\left(\frac{m}{u_0}\right) + \frac{64i\pi^2\alpha_3^2\beta^2}{q^2} - \frac{32i\pi^2\alpha_3^2\beta^2}{q} + 8i\pi\alpha_3^4\beta^2 B_{0z}^2 - 16i\pi^2\alpha_3^2\beta^4. \tag{14}$$

A. Without magnetic field

To extract the hydrodynamical effect out of Eq. (14), we set $B_{0z} = 0$. Then, the corresponding dispersion relation becomes

$$-i\alpha_3^2\beta^2 + \frac{m}{u_0}\beta + \frac{2\alpha_3}{q}\left(\frac{m}{u_0}\right) + \frac{4i\alpha_3^2}{q^2} - \frac{2i\alpha_3^2}{q} = 0. \tag{15}$$

The solutions of this quadratic equation are

$$\beta = \frac{1}{2\alpha_3^2}\left[-i\left(\frac{m}{u_0}\right) \pm \sqrt{\frac{8\alpha_3^4}{q^2}(2-q) - \frac{m}{u_0}\left(\frac{m}{u_0} + \frac{8i\alpha_3^3}{q}\right)}\right]. \tag{16}$$

If we compare Eq. (16) with Eq. (11), we note the effect of noise on the stability of the flow. Equation (16) has two solutions. However, only one of them gives us positive $Im(\beta)$ as a function of m/u_0, i.e., only that particular solution corresponds to instability in the flow. As we are interested in instability, we consider the first solution. In this case, the positive sign in front of the square root corresponds to the unstable solution.

Figure 2 describes the variation of $Im(\beta)$ from Eq. (16) as a function of m/u_0 for various combinations of q and α_3. Here, we note that for positive m/u_0, when α_3 has been kept fixed, $Im(\beta)$ reaches a maximum and then it decreases. The maximum decreases as q decreases. Apart from that, the value of m/u_0, at which the maximum in $Im(\beta)$ occurs, increases as q decreases. It, indeed, should be the case. Now, for the negative m/u_0, for the same case, it is obvious from the inset that the curve of larger q is steeper. It means that at each negative m/u_0, larger q has larger $Im(\beta)$. This is what is expected. From Eq. (11), when the force is zero, $q = 2$ gives the marginal stability and $q < 2$ makes the flow stable and the stability increases as q becomes lesser than 2. A lesser q, therefore, takes a larger force to make the flow unstable. For a fixed q, as α_3 increases, the curves become less steeper in most of the cases; hence, at each m/u_0, a lesser α_3 has a larger growth rate $[Im(\beta)]$. This nature of the growth rate for negative m/u_0 is quite obvious from Eq. (16). However, for the positive m/u_0, we note that there will be a competition between the terms with and without square root in Eq. (16). As a result, for $\alpha_3 = 1$ and $q = 1.5$, we see that the growth rate increases as m/u_0 increases up to a certain value of m/u_0. Beyond that certain m/u_0, the growth rate decreases.

B. With magnetic field

Equation (14) is a quartic equation. Here, we look for the imaginary part of each root. Among the four solutions,

- the first and the fourth solutions together give us the solution given by Eq. (16) when the magnetic field is switched off,
- the third solution gives us the MRI modes when noise is not there in the flow, and
- the second solution gives us the stable modes corresponding to the MRI modes if the noise is made zero.

We will begin with the "third solution" as it reduces to the usual MRI mode shown in Fig. 1 when there is no noise in the system.

1. The "third solution"

Figure 3 describes the variation of $Im(\beta)$ as a function of m/u_0 and B_{0z} for $q = 1.5$ and $\alpha_3 = 1$. From Fig. 1, it is clear that for $q = 1.5$ and $\alpha_3 = 1$, the domain of B_{0z} that gives rise to positive $Im(\beta)$ is about within -4 to $+4$. To see what happens in that region of B_{0z}, we fix the range of the vertical axis in Fig. 3 within -5 to $+5$. We note that the growth rate is mostly dominated by MRI in that region of the magnetic field. Around $m/u_0 = 0$, as the magnitude of B_{0z} increases, $Im(\beta)$ increases initially, reaches a maximum, and then again decays. In addition, beyond a small region around $|m/u_0| = 0$, the flow is stable within the domain of m/u_0 as shown in Fig. 3. However, the maximum growth rate shown in this figure is greater than the MRI growth rate shown in Fig. 1. This could be due to the additional effect from the hydrodynamic instability because of the presence of noise in the flow.

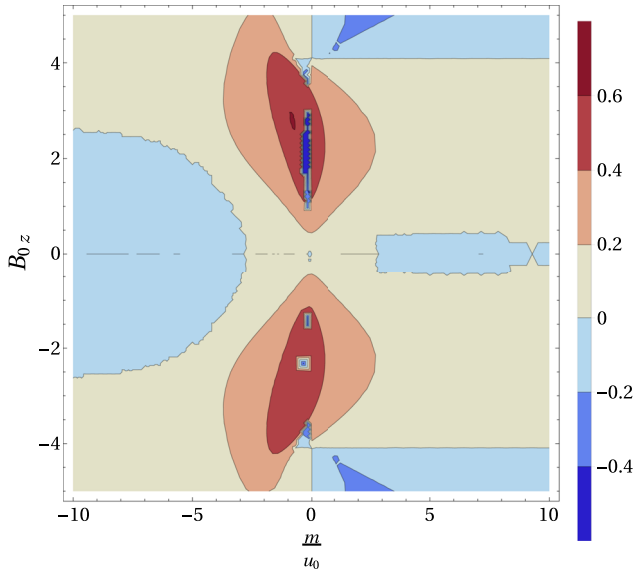

FIG. 3. Variation of $Im(\beta)$ of the "third solution" of Eq. (14) as described in Sec. IV B as a function of m/u_0 and B_{0z} for $q = 1.5$ and $\alpha_3 = 1$ for inviscid flow.

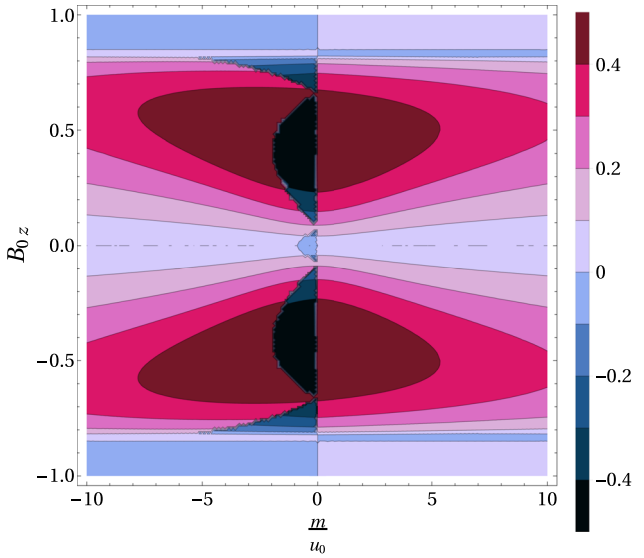

FIG. 5. Variation of $Im(\beta)$ of the "third solution" of Eq. (14) as described in Sec. IV B as a function of m/u_0 and B_{0z} in for $q = 1.5$ and $\alpha_3 = 5$ for inviscid flow.

Now, if we increase the domain of m/u_0 and B_{0z}, we note that the flow is mostly stable for positive m/u_0, but it is mostly unstable for negative m/u_0, as indicated by Fig. 4, where the variation of $Im(\beta)$ is shown as a function of m/u_0 and B_{0z} in the larger domain. As the magnitude of m/u_0 increases, we note that the growth rate increases. However, the positive growth rate becomes almost independent of the magnetic field at large m/u_0. That is to say, at the larger magnetic field where there is no growth due to MRI, the flow is mostly governed by the noise with huge growth rates.

Now, we increase α_3 to 5. Figure 5 shows the variation of $Im(\beta)$ as a function of m/u_0 and B_{0z} for $q = 1.5$ and $\alpha_3 = 5$. From Fig. 1, we already have obtained that for $q = 1.5$ and $\alpha_3 = 5$, the window of B_{0z} that gives rise to positive $Im(\beta)$ is about within −1 to +1. We, therefore, keep the range of the vertical axis in Fig. 5 within ±1 so that we can compare between MRI and instability due to noise. There,

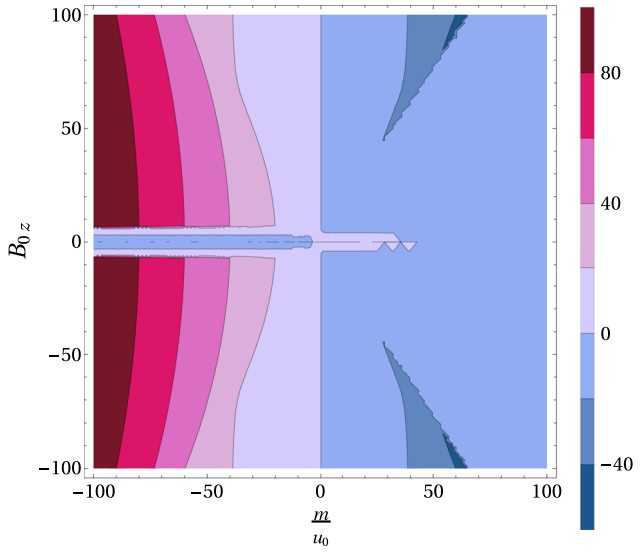

FIG. 4. Variation of $Im(\beta)$ of the "third solution" of Eq. (14) as described in Sec. IV B as a function of m/u_0 and B_{0z} in the larger domain for $q = 1.5$ and $\alpha_3 = 1$ for inviscid flow.

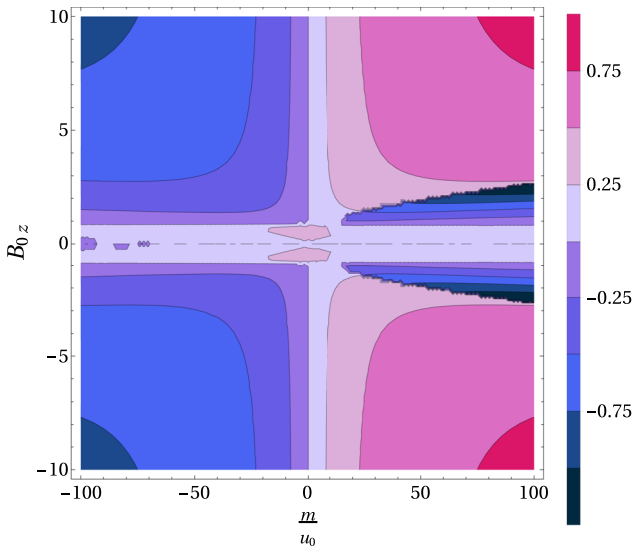

FIG. 6. Variation of $Im(\beta)$ of the "third solution" of Eq. (14) as described in Sec. IV B as a function of m/u_0 and B_{0z} in the larger domain for $q = 1.5$ and $\alpha_3 = 5$ for inviscid flow.

we note that the growth rate is mostly governed by the MRI, and the structure of the growth rate, i.e., how $Im(\beta)$ varies with B_{0z} at a particular m/u_0, is also MRI-like. If we compare between Figs. 3 and 5, we observe that the range of $|m/u_0|$, which gives rise to a positive growth rate, increases as α_3 increases.

Now, let us see what happens to the growth rates when we extend the domain of m/u_0 and B_{0z} through Fig. 6, where the variation of $Im(\beta)$ has been shown as a function of m/u_0 and B_{0z} for $q = 1.5$ and $\alpha_3 = 5$. There, we note that for negative m/u_0, the flow is stable for any magnetic field. On the other hand, for positive m/u_0, the flow is mostly unstable. However, there is a window of $-3 \lesssim B_{0z} \lesssim +3$, where the flow could be stable depending on m/u_0. Here, noise has the stabilizing effect because if we fix the magnetic field at any value within ± 3, we note that the flow suddenly becomes stable as we increase m/u_0. However, in the unstable region, as the noise increases, the growth rate increases, and ultimately at large noise, the instability, due to the noise, takes over the flow. Thus, the regime of the sterile magnetic field not leading to MRI, i.e., the strong field, turns out to be active in order to reveal instability in the presence of noise.

Now, we further increase α_3 to 10, which is, in fact, very much applicable to the accretion flow.[37] Figure 7 describes the variation of $Im(\beta)$ as a function of m/u_0 and B_{0z} for $q = 1.5$ and $\alpha_3 = 10$. We bound the vertical axis within ± 0.5 in this figure as Fig. 1 shows that the range of B_{0z} that gives rise to a positive growth rate is within around ± 0.5. Here again, we note that in this domain of magnetic field, the growth rate is mostly dominated by MRI. However, in comparison with the other two α_3, for $\alpha_3 = 10$, the range of m/u_0, which gives rise to a positive growth rate, is larger. Nevertheless, for the larger magnetic field, where MRI is inactive, the flow is again dominated by the instability due to the noise, particularly for positive m/u_0. This phenomenon is well-depicted in Fig. 8, which shows the variation of $Im(\beta)$ as a function of m/u_0 and B_{0z} in the larger domain for $q = 1.5$ and $\alpha_3 = 10$.

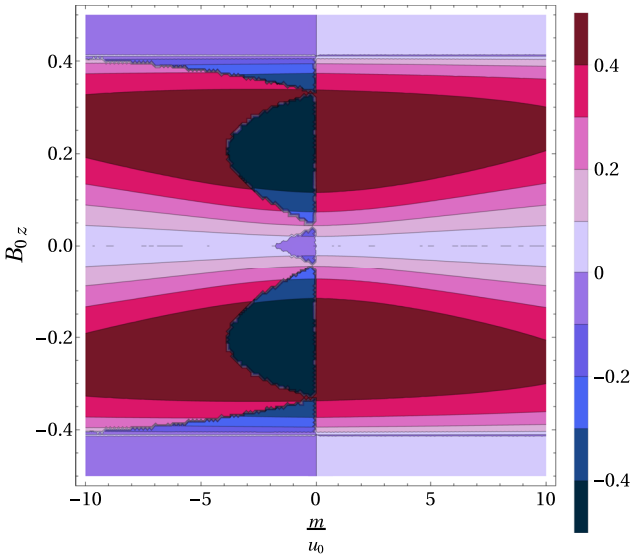

FIG. 7. Variation of $Im(\beta)$ of the "third solution" of Eq. (14) as described in Sec. IV B as a function of m/u_0 and B_{0z} for $q = 1.5$ and $\alpha_3 = 10$ for inviscid flow.

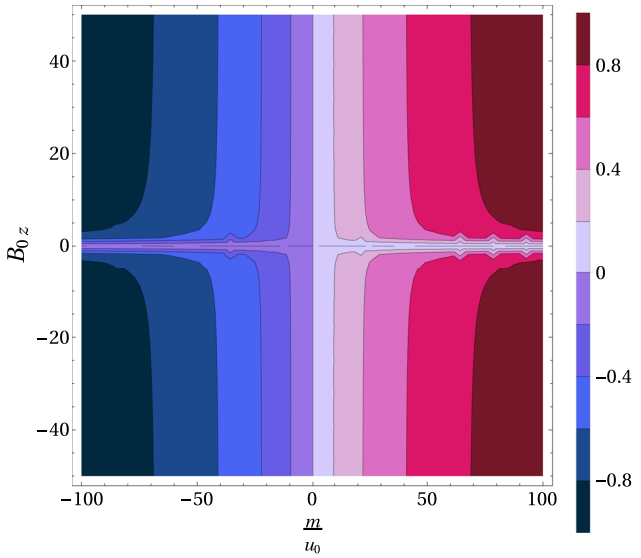

FIG. 8. Variation of $Im(\beta)$ of the "third solution" of Eq. (14) as described in Sec. IV B as a function of m/u_0 and B_{0z} in the larger domain for $q = 1.5$ and $\alpha_3 = 10$ for inviscid flow.

2. The "first solution"

The "first solution" of $Im(\beta)$ from Eq. (14) as described in Sec. IV B is shown in Fig. 9 for $B_{0z} = 0$ and three different α_3. There, we note that the variation of $Im(\beta)$ for positive m/u_0 is the same as of Fig. 2 for positive m/u_0. We see that up to certain positive m/u_0, the growth rates corresponding to the smaller α_3 increase steeply. However, beyond that m/u_0, the growth rate decreases. The similar feature is depicted in Fig. 10 where the variation of the growth rate is shown a function of m/u_0 and B_{0z} for $\alpha_3 = 1$. However, for a particular m/u_0, we see that the growth rate decreases with the increase in the magnitude of B_{0z}. Hence, in this case, the magnetic field affects the flow destructively with the effect of noise.

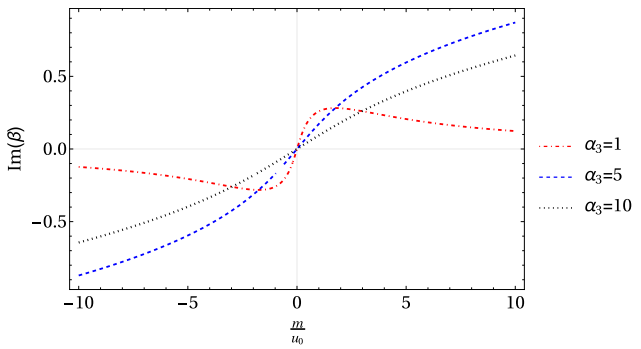

FIG. 9. Variation of $Im(\beta)$ of the "first solution" of Eq. (14) as described in Sec. IV B as a function of m/u_0 for $q = 1.5$ and three different α_3 when $B_{0z} = 0$ for inviscid flow.

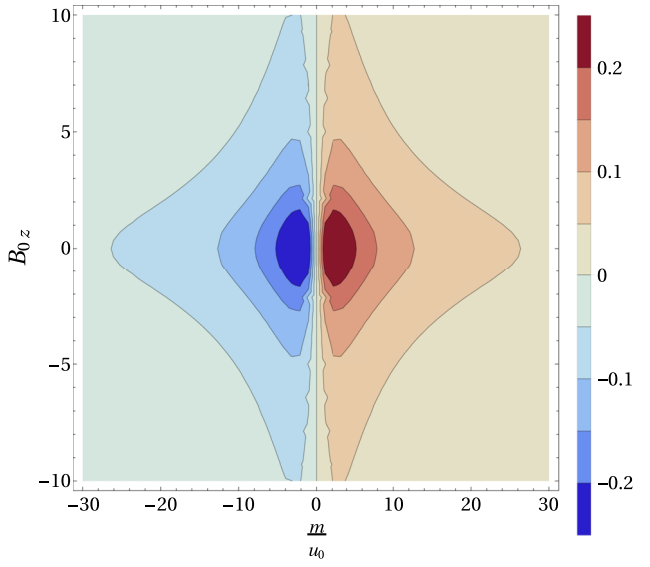

FIG. 10. Variation of $Im(\beta)$ of the "first solution" of Eq. (14) as described in Sec. IV B as a function of m/u_0 and B_{0z} for $q = 1.5$ and $\alpha_3 = 1$ for inviscid flow.

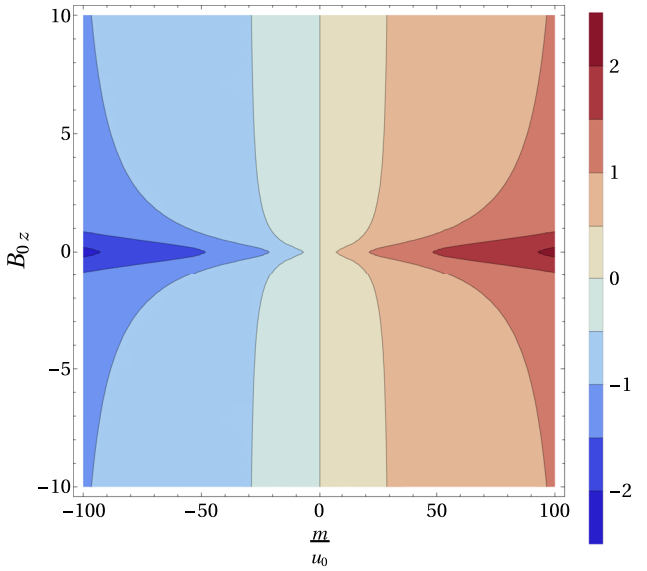

FIG. 12. Variation of $Im(\beta)$ of the "first solution" of Eq. (14) as described in Sec. IV B as a function of m/u_0 and B_{0z} for $q = 1.5$ and $\alpha_3 = 10$ for inviscid flow.

Figures 11 and 12 show the variation of $Im(\beta)$ of the "first solution" of Eq. (14) as described in Sec. IV B as a function of m/u_0 and B_{0z} for $q = 1.5$ for $\alpha_3 = 5$ and 10, respectively. There, we note that the growth rates for these two cases are similar to that in Fig. 10. Within a very small domain of the magnetic field, for a fixed m/u_0, the growth rate decreases with the increase in the magnitude of the magnetic field. Beyond that domain of B_{0z}, the growth rate is almost independent of the magnetic field. However, the domain of the magnetic field, in which the growth rate depends on the magnetic field, shrinks in size as α_3 increases from 5 to 10. It could plausibly be because nonzero noise effectively brings in MRI-like features, i.e., the decrease in size of the MRI active magnetic field regime due to the increase in wavevector for a particular region of the magnetic field.

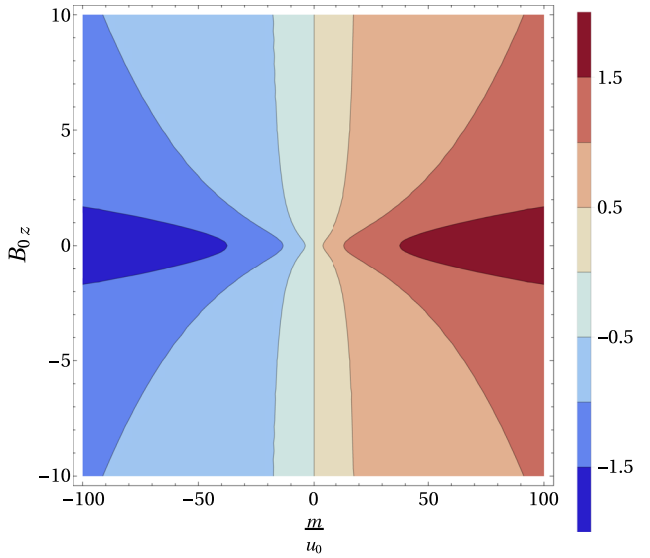

FIG. 11. Variation of $Im(\beta)$ of the "first solution" of Eq. (14) as described in Sec. IV B as a function of m/u_0 and B_{0z} for $q = 1.5$ and $\alpha_3 = 5$ for inviscid flow.

The maximum growth rate in Fig. 12 is relatively larger than that in Fig. 8. Note that both of these figures have the same α_3 and the same range of m/u_0. While Fig. 8 represents the "third solution" for a given set of parameters, Fig. 12 represents the "first solution" for the concerned parameters. The latter one, being solely hydrodynamical, does not have any MRI counterpart. On the contrary, the former one does reduce to the MRI solution at the vanishing noise.

3. The "second solution"

The "second solution" of Eq. (14) is the stable version of the third solution of the same equation if there is no noise in the flow. Figure 13 shows the variation of $Im(\beta)$ of the second solution of Eq. (14) as a function of m/u_0 and B_{0z} for $q = 1.5$ and $\alpha_3 = 10$. Figure 14 also depicts the same but in the larger domain of m/u_0 and B_{0z}. We note that Fig. 13 is almost complementary to Fig. 6. Within a certain domain of B_{0z}, the flow is stable, and the stability arises due to the domination of the magnetic field over the effect of noise. However, beyond that particular domain of B_{0z}, the flow becomes unstable due the effect of noise. For negative m/u_0, we note that beyond certain magnetic field, the growth rate increases as the magnitude of m/u_0 increases. In this region, the growth rate increases with the increase in magnitude of both m/u_0 and B_{0z}. However, at the larger magnetic field, the flow is almost controlled by the noise, particularly with negative mean. We are also familiar with similar invasion of noise but with positive mean in the case of the third solution described in Sec. IV B 1.

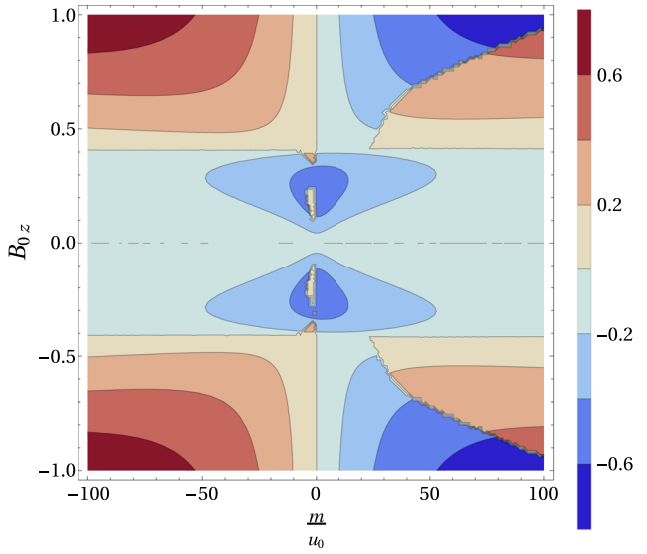

FIG. 13. Variation of $Im(\beta)$ of the "second solution" of Eq. (14) as described in Sec. IV B as a function of m/u_0 and B_{0z} for $q = 1.5$ and $\alpha_3 = 10$ for inviscid flow.

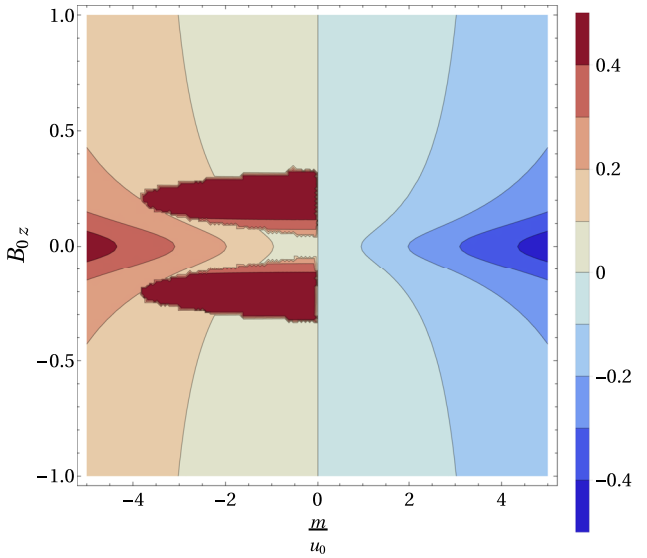

FIG. 15. Variation of $Im(\beta)$ of the "fourth solution" of Eq. (14) as described in Sec. IV B as a function of m/u_0 and B_{0z} for $q = 1.5$ and $\alpha_3 = 10$ for inviscid flow.

4. The "fourth solution"

The "fourth solution" of Eq. (14) is the almost complementary solution to the first solution of the same equation. However, there is some difference, i.e., they are not exactly the complex conjugate as the coefficients of Eq. (14) are complex quantities. It will be understood if we go through Fig. 15, which describes variation of $Im(\beta)$ of the fourth solution of Eq. (14) as a function of m/u_0 and B_{0z} in the larger domain for $q = 1.5$ and $\alpha_3 = 10$. Here, we note that for negative m/u_0, the growth rate is positive. For smaller m/u_0, as the magnitude of the magnetic field increases, only up to a certain range of the magnetic field, the growth rate increases. However, for the lager m/u_0, the above phenomenon reverses, i.e., as the magnitude of the magnetic field increases, the flow becomes less unstable. Now, for the larger ranges of m/u_0 and B_{0z}, as described by Fig. 16, it is the noise that takes over the flow. Consequently, the instability in the flow arises due to the noise.

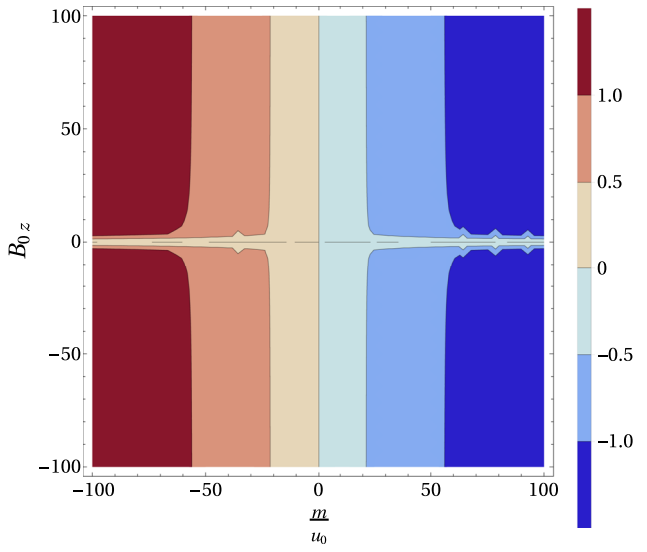

FIG. 14. Variation of $Im(\beta)$ of the "second solution" of Eq. (14) as described in Sec. IV B as a function of m/u_0 and B_{0z} in the larger domain for $q = 1.5$ and $\alpha_3 = 10$ for inviscid flow.

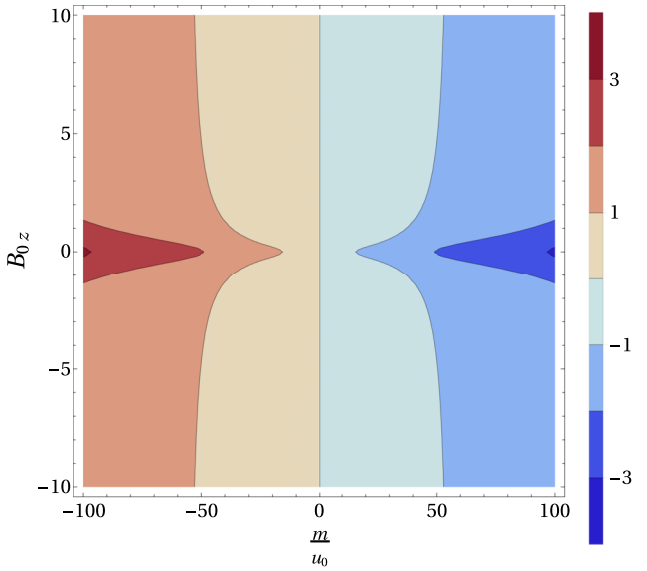

FIG. 16. Variation of $Im(\beta)$ of the "fourth solution" of Eq. (14) as described in Sec. IV B as a function of m/u_0 and B_{0z} in the larger range for $q = 1.5$ and $\alpha_3 = 10$ for inviscid flow.

V. THE EFFECT OF *RE*

Untill now, we have not considered the effect of viscous dissipation. Let us explore the effect of the same on the growth rates. Consequently, Eq. (13) becomes

$$\begin{aligned}
&\left(i\beta\alpha_3^2 - \frac{\alpha^4}{Re}\right)u(0) + \frac{2i\alpha_3}{q}\zeta(0) + \frac{i\alpha_3^3 B_{0z}B_x(0)}{4\pi} = m_1,\\
&i\alpha_3\left(1-\frac{2}{q}\right)u(0) + \left(\frac{\alpha^2}{Re} - i\beta\right)\zeta(0) - \frac{i}{4\pi}B_{0z}\alpha_3\zeta_B(0) = m_2,\\
&-i\beta B_x(0) - iB_{0z}\alpha_3 u(0) = 0,\\
&-i\beta\zeta_B(0) - iB_{0z}\alpha_3\zeta(0) - i\alpha_3 B_x(0) = 0.
\end{aligned} \tag{17}$$

The corresponding dispersion relation for $m_1 = m_2 = m$ from Eq. (17) becomes

$$\begin{aligned}
&\frac{m}{u_0}\left(4\pi\alpha_3^2 B_{0z}^2\beta - \frac{16i\pi^2\alpha_3^2\beta^2}{Re} - 16\pi^2\beta^3\right)\\
&= \frac{8i\pi B_{0z}^2\alpha_3^4}{q} - i\alpha_3^6 B_{0z}^4 + \frac{32\pi^2\alpha_3\beta^2}{q}\left(\frac{m}{u_0}\right) + \frac{64i\pi^2\alpha_3^2\beta^2}{q^2}\\
&\quad - \frac{32i\pi^2\alpha_3^2\beta^2}{q} + 8i\pi\alpha_3^4\beta^2 B_{0z}^2 + \frac{16i\pi^2\alpha_3^6\beta^2}{Re^2} + \frac{32\pi^2\alpha_3^4\beta^3}{Re}\\
&\quad - 16i\pi^2\alpha_3^2\beta^4.
\end{aligned} \tag{18}$$

If the magnetic field is not there in the system, then the above dispersion relation becomes

$$\begin{aligned}
&-i\alpha_3^2\beta^2 + \left(\frac{2\alpha_3^4}{Re} + \frac{m}{u_0}\right)\beta + \frac{2\alpha_3}{q}\left(\frac{m}{u_0}\right)\\
&\quad + \frac{4i\alpha_3^2}{q^2} - \frac{2i\alpha_3^2}{q} + \frac{i\alpha_3^2}{Re}\left(\frac{m}{u_0}\right) + \frac{i\alpha_3^6}{Re^2} = 0
\end{aligned} \tag{19}$$

with the solutions

$$\beta = \frac{1}{2\alpha_3^2}\left[-i\left(\frac{m}{u_0}\right) - \frac{2i\alpha_3^4}{Re} \pm \sqrt{\frac{8\alpha_3^4}{q^2}(2-q) - \frac{m}{u_0}\left(\frac{m}{u_0} + \frac{8i\alpha_3^3}{q}\right)}\right]. \tag{20}$$

If we compare Eq. (16) with Eq. (20), we note that the latter has an additional term involving *Re*. Since the term is imaginary, it reduces the instability in the flow. Hence, inclusion of *Re* makes the flow less unstable if there is no effect of magnetic field in the flow. Equation (19) is the same as Eq. (9) in Ref. 35. Figure 2 in Ref. 35 also suggests that inclusion of *Re* decreases the growth rate.

Let us incorporate the magnetic field in the flow and get rid of the effect of noise. Then, we obtain the usual MRI but with the effect of viscosity. Figure 17 shows the variation of $Im(\beta)$ of the third solution of Eq. (18) when $m = 0$ as a function of B_{0z} for $q = 1.5$, $\alpha_3 = 10$, and $Re = 100, 200,$ and 500. This figure shows that with the inclusion of viscosity, i.e., *Re* in the flow, the growth rate decreases. As *Re* increases, the corresponding growth rates also increase and ultimately reach the results of the inviscid limit. This phenomenon

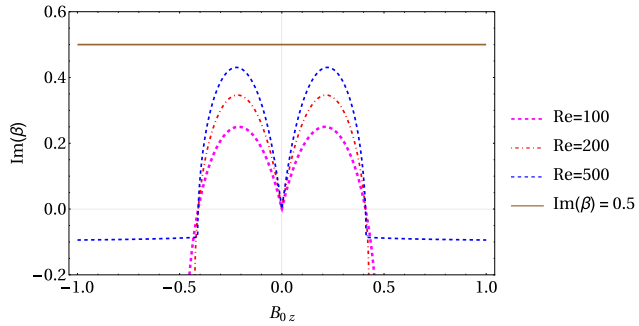

FIG. 17. Variation of $Im(\beta)$ of the third solution of Eq. (18) when $m = 0$ as a function of B_{0z} for $q = 1.5$, $\alpha_3 = 10$, and $Re = 100, 200,$ and 500.

becomes obvious once we compare between Figs. 17 and 1. Let us study the effect of *Re* on the growth rate if both magnetic field and the noise are present in the flow. Figure 18 shows the variation of $Im(\beta)$ of the third solution of Eq. (18) as a function of m/u_0 and B_{0z} for $q = 1.5$, $\alpha_3 = 10$, and $Re = 100$. If we compare Figs. 8 and 18, we note that in the latter case, the growth rate decreases due to considering the viscosity, i.e., *Re* in the flow.

Figure 19 shows the variation of $Im(\beta)$ of the first solution of Eq. (18) as a function of m/u_0 and B_{0z} for $q = 1.5$, $\alpha_3 = 10$, and $Re = 50$. If we compare it with Fig. 12, we note that the growth rate becomes negative, i.e., the flow becomes stable, for $Re = 50$. However, as *Re* increases, the growth rates increases and eventually at large *Re*, Fig. 19 becomes Fig. 12. Now, $Im(\beta)$ for the second and fourth solutions of Eq. (18) also get reduced due the presence of the viscosity, i.e., *Re*.

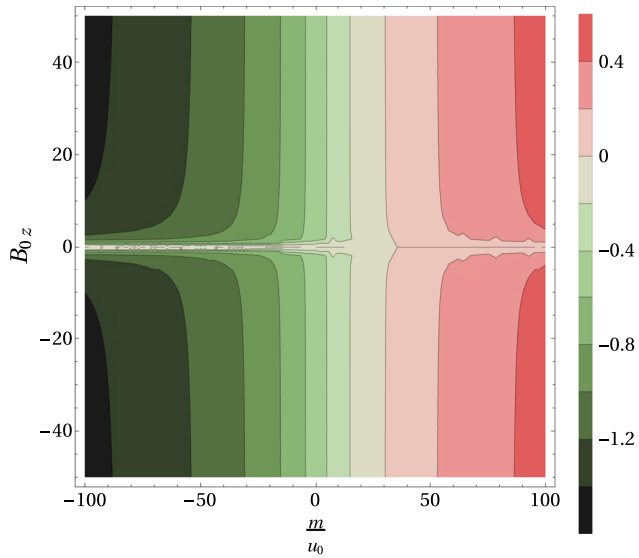

FIG. 18. Variation of $Im(\beta)$ of the third solution of Eq. (18) as a function of m/u_0 and B_{0z} for $q = 1.5$, $\alpha_3 = 10$, and $Re = 100$.

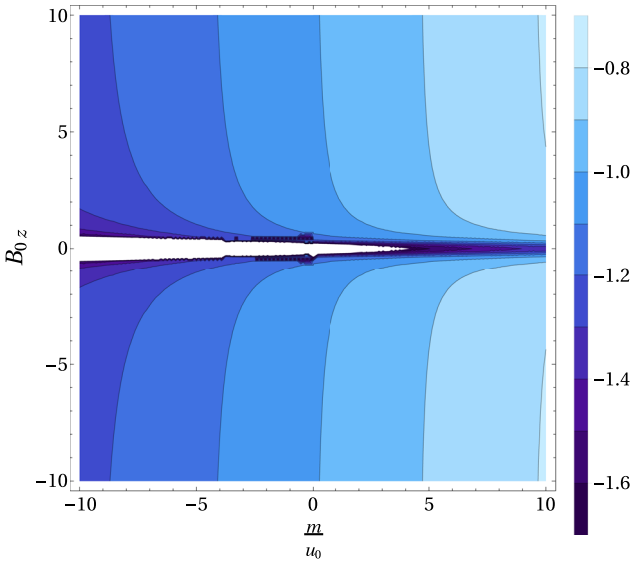

FIG. 19. Variation of $Im(\beta)$ of the first solution of Eq. (18) as a function of m/u_0 and B_{0z} for $q = 1.5$, $\alpha_3 = 10$, and $Re = 50$.

VI. CONCLUSION

The transport of angular momentum outward and that of the matter inward in the accretion disk are still debatable and arguably open question until today, particularly at the low-temperature region of the accretion disks. In the hot region, MRI is quite successful in explaining the transport. However, there are different parameter regimes (e.g., large magnetic field and huge Reynolds number,[14] a large toroidal component of the magnetic field,[13] etc.) where MRI gets suppressed or ceases to work. In the previous publications,[36–38] we attempted to propose a generic instability mechanism from the hydrodynamical point of view if noise is present in the corresponding flow. With that thought, here we have attempted to compare the growth rates corresponding to both the mechanisms. We have attempted to check what happens to the growth rates if both magnetic field and the noise with non-zero mean are present in the flow. From the analysis, our conclusions are given as follows:

- Among the four solutions for the growth rates, one of them reduces to the MRI growth rate if the noise is absent. If both noise and the magnetic field are present in the flow, in the MRI active region of the magnetic field, the growth rates follow the MRI growth rate pattern, i.e., the growth rate first increases, attain a maximum, and then again decrease with the variation of magnetic field. However, the corresponding maximum growth rate is slightly larger than the MRI growth rate. In the larger domain of magnetic field where MRI is inactive, the instability is almost entirely due to the noise as the corresponding growth rates are almost independent of the magnetic field. However, there is another growth rate that is almost complementary to the above-mentioned growth rate.
- Furthermore, there is another solution for the growth rate that reduces to the growth rate related to the hydrodynamic instability due to the presence of noise in the flow when the magnetic field is absent. This solution has nothing to do with MRI. When both the magnetic field and noise are retained in the flow, at the MRI active magnetic field region, also the growth rate is larger than that of the MRI. This growth rate does not have any MRI imprint. The magnitude of the growth rate mostly depends on the mean of the noise. As the mean increases, the growth rate increases. However, this also has an almost complementary growth rate, which is the last solution in the set of four.
- The above points summarize that even in the MRI active region, as there are two growth rates that are larger at the comparatively larger mean of the noise than those of the other two solutions that have the imprint of MRI, the corresponding flow becomes unstable due to the hydrodynamical instability in the presence of noise.
- All the growth rates decrease due to the presence of viscosity in the flow. As the Reynolds number increases, the corresponding growth rates increase, as expected.

ACKNOWLEDGMENTS

S.G. acknowledges DST India for INSPIRE fellowship. We would like to thank Professor Vinod Krishan of the Indian Institute of Astrophysics for her constructive comments and suggestions that helped to shape our thoughts in better ways. This work was partly supported by a fund of the Department of Science and Technology (DST-SERB) under Research Grant No. DSTO/PPH/BMP/1946 (EMR/2017/001226) and a fund of the Indian Institute of Science.

AUTHOR DECLARATIONS

Conflict of Interest

The authors have no conflicts to disclose.

DATA AVAILABILITY

The data that support the findings of this study are available from the corresponding author upon reasonable request.

REFERENCES

[1] J. Frank, A. King, and D. J. Raine, in *Accretion power in Astrophysics*, edited by J. Frank, A. King, and D. Raine (Cambridge, UK: Cambridge University Press, 2002), ISBN: 0521620538, p. 398.
[2] N. I. Shakura and R. A. Sunyaev, "Black holes in binary systems. Observational appearance," Astron. Astrophys. **24**, 337–355 (1973).
[3] S. A. Balbus and J. F. Hawley, "A powerful local shear instability in weakly magnetized disks. I-Linear analysis," Astrophys. J. **376**, 214–233 (1991).
[4] E. Velikhov, "Stability of an ideally conducting liquid flowing between rotating cylinders in a magnetic field," Zh. Eksp. Teor. Fiz. **36**, 1398 (1959).
[5] S. Chandrasekhar, "The stability of non-dissipative Couette flow in hydromagnetics," Proc. Natl. Acad. Sci. **46**, 253–257 (1960).
[6] S. A. Balbus and J. F. Hawley, "Instability, turbulence, and enhanced transport in accretion disks," Rev. Mod. Phys. **70**, 1–53 (1998).
[7] C. F. Gammie, "Layered accretion in T tauri disks," Astrophys. J. **457**, 355 (1996).
[8] T. Fleming and J. M. Stone, "Local magnetohydrodynamic models of layered accretion disks," Astrophys. J. **585**, 908–920 (2003); arXiv:astro-ph/0210541 [astro-ph].

[9]N. J. Turner, S. Fromang, C. Gammie, H. Klahr, G. Lesur, M. Wardle, and X. N. Bai, "Transport and accretion in planet-forming disks," in Protostars and Planets VI, edited by H. Beuther, R. S. Klessen, C. P. Dullemond, and T. Henning (University of Arizona Press, 2014), p. 411; arXiv:1401.7306 [astro-ph.EP].
[10]X.-N. Bai and J. M. Stone, "Wind-driven accretion in protoplanetary disks. I. Suppression of the magnetorotational instability and launching of the magneto-centrifugal wind," Astrophys. J. **769**, 76 (2013); arXiv:1301.0318 [astro-ph.EP].
[11]X.-N. Bai, "Wind-driven accretion in protoplanetary disks. II. Radial dependence and global picture," Astrophys. J. **772**, 96 (2013); arXiv:1305.7232 [astro-ph.EP].
[12]M. E. Pessah and D. Psaltis, "The stability of magnetized rotating plasmas with superthermal fields," Astrophys. J. **628**, 879–901 (2005); arXiv:astro-ph/0406071.
[13]U. Das, M. C. Begelman, and G. Lesur, "Instability in strongly magnetized accretion discs: A global perspective," Mon. Not. R. Astron. Soc. **473**, 2791–2812 (2018); arXiv:1709.09173 [astro-ph.HE].
[14]S. K. Nath and B. Mukhopadhyay, "Origin of nonlinearity and plausible turbulence by hydromagnetic transient growth in accretion disks: Faster growth rate than magnetorotational instability," Phys. Rev. E **92**, 023005 (2015); arXiv:1505.02874 [astro-ph.HE].
[15]B. Mukhopadhyay and A. K. Chattopadhyay, "Stochastically driven instability in rotating shear flows," J. Phys. A: Math. Gen. **46**, 035501 (2013); arXiv:1211.5135 [astro-ph.HE].
[16]S. Chandrasekhar, *Hydrodynamic and Hydromagnetic Stability* (Oxford University Press, 1961).
[17]L. D. Landau and E. M. Lifshitz, *Fluid Mechanics* (Pergamon Press, 1959).
[18]D. Richard and J.-P. Zahn, "Turbulence in differentially rotating flows what can be learned from the Couette–Taylor experiment," Astron. Astrophys. **347**, 734–738 (1999); arXiv:astro-ph/9903374 [astro-ph].
[19]D. P. M. van Gils, G.-W. Bruggert, D. P. Lathrop, C. Sun, and D. Lohse, "The twente turbulent taylor–couette (T^3C) facility: Strongly turbulent (multiphase) flow between two independently rotating cylinders," Rev. Sci. Instrum. **82**, 025105 (2011).
[20]M. S. Paoletti and D. P. Lathrop, "Angular momentum transport in turbulent flow between independently rotating cylinders," Phys. Rev. Lett. **106**, 024501 (2011).
[21]M. S. Paoletti, D. P. M. van Gils, B. Dubrulle, C. Sun, D. Lohse, and D. P. Lathrop, "Angular momentum transport and turbulence in laboratory models of Keplerian flows," Astron. Astrophys. **547**, A64 (2012).
[22]H. Ji, M. Burin, E. Schartman, and J. Goodman, "Hydrodynamic turbulence cannot transport angular momentum effectively in astrophysical disks," Nature **444**, 343–346 (2006); arXiv:astro-ph/0611481 [astro-ph].
[23]S. Fromang and G. Lesur, "Angular momentum transport in accretion disks: A hydrodynamical perspective," *EAS Publications Series* (EDP Sciences, 2019), Vol. 82, pp. 391–413.
[24]M. Avila, "Stability and angular-momentum transport of fluid flows between corotating cylinders," Phys. Rev. Lett. **108**, 124501 (2012); arXiv:1203.4923 [physics.flu-dyn].
[25]A. G. Tevzadze, G. D. Chagelishvili, J.-P. Zahn, R. G. Chanishvili, and J. G. Lominadze, "On hydrodynamic shear turbulence in stratified Keplerian disks: Transient growth of small-scale 3D vortex mode perturbations," Astron. Astrophys. **407**, 779–786 (2003).
[26]G. D. Chagelishvili, J.-P. Zahn, A. G. Tevzadze, and J. G. Lominadze, "On hydrodynamic shear turbulence in Keplerian disks: Via transient growth to bypass transition," Astron. Astrophys. **402**, 401–407 (2003).
[27]P. A. Yecko, "Accretion disk instability revisited: Transient dynamics of rotating shear flow," Astron. Astrophys. **425**, 385–393 (2004).
[28]B. Mukhopadhyay, N. Afshordi, and R. Narayan, "Bypass to turbulence in hydrodynamic accretion disks: An eigenvalue approach," Astrophys. J. **629**, 383–396 (2005); arXiv:astro-ph/0412193.
[29]N. Afshordi, B. Mukhopadhyay, and R. Narayan, "Bypass to turbulence in hydrodynamic accretion: Lagrangian analysis of energy growth," Astrophys. J. **629**, 373–382 (2005); arXiv:astro-ph/0412194.
[30]P. J. Schmid, D. S. Henningson, and D. F. Jankowski, "Stability and transition in shear flows," Appl. Mech. Rev. **55**, B57–B59 (2002).
[31]G. Lesur and P.-Y. Longaretti, "On the relevance of subcritical hydrodynamic turbulence to accretion disk transport," Astron. Astrophys. **444**, 25–44 (2005).
[32]L. Shi, B. Hof, M. Rampp, and M. Avila, "Hydrodynamic turbulence in quasi-Keplerian rotating flows," Phys. Fluids **29**, 044107 (2017); arXiv:1703.01714 [physics.flu-dyn].
[33]P. J. Ioannou and A. Kakouris, "Stochastic dynamics of Keplerian accretion disks," Astrophys. J. **550**, 931–943 (2001).
[34]D. N. Razdoburdin, "Perturbation dynamics in Keplerian flow under external stochastic forcing," Mon. Not. R. Astron. Soc. **492**, 5366–5376 (2020).
[35]S. K. Nath and B. Mukhopadhyay, "A pure hydrodynamic instability in shear flows and its application to astrophysical accretion disks," Astrophys. J. **830**, 86 (2016); arXiv:1608.00980 [astro-ph.HE].
[36]S. Ghosh and B. Mukhopadhyay, "Hydrodynamical instability with noise in the Keplerian accretion discs: Modified Landau equation," Mon. Not. R. Astron. Soc. **496**, 4191–4208 (2020).
[37]S. Ghosh and B. Mukhopadhyay, "Origin of hydrodynamic instability from noise: From laboratory flow to accretion disk," Phys. Rev. Fluids **6**, 013903 (2021); arXiv:2012.13417 [astro-ph.HE].
[38]S. Ghosh and B. Mukhopadhyay, "Forced linear shear flows with rotation: Rotating Couette–Poiseuille flow, its stability and astrophysical implications," Astrophys. J. **922**(2), 161 (2021).
[39]T. Singh Bhatia and B. Mukhopadhyay, "Exploring non-normality in magneto-hydrodynamic rotating shear flows: Application to astrophysical accretion disks," Phys. Rev. Fluids **1**, 063101 (2016); arXiv:1609.01841 [astro-ph.HE].
[40]B. Mukhopadhyay, R. Mathew, and S. Raha, "Growing pseudo-eigenmodes and positive logarithmic norms in rotating shear flows," New J. Phys. **13**, 023029 (2011); arXiv:1101.4608 [astro-ph.HE].
[41]P. G. Drazin and W. H. Reid, *Hydrodynamic Stability*, edited by P. G. Drazin and W. H. Reid (Cambridge, UK: Cambridge University Press, 2004), ISBN: 0521525411, p. 626.